

Core shift in parabolic accelerating jets

E. E. Nokhrina^{1,2*}, A. B. Pushkarev^{3,1}

¹*Lebedev Physical Institute, Leninsky prosp. 53, Moscow, 119991, Russia*

²*Moscow Institute of Physics and Technology, Dolgoprudny, Institutsky per., 9, Moscow region, 141700, Russia*

³*Crimean Astrophysical Observatory, Nauchny 298688, Crimea, Russia*

Accepted 2024 January 11. Received 2024 January 11; in original form 2023 September 28

ABSTRACT

The core shift method is a powerful method to estimate the physical parameters in relativistic jets from active galactic nuclei. The classical approach assumes a conical geometry of a jet and a constant plasma speed. However, recent observations showed that neither may hold close to the central engine, where plasma in a jet is effectively accelerating, and the jet geometry is quasi-parabolic. We modify the classical core shift method to account for these jet properties. We show that the core shift index may assume values in the range 0.8 – 1.2 or 0.53 – 0.8 depending on the jet geometry and viewing angle, with the indices close to both values are indeed being observed. We obtain the expressions to estimate jet magnetic field and a total magnetic flux in a jet. We show that the obtained magnetic field value can be easily recalculated down to the gravitational radius scales. For M 87 and NGC 315 these values are in good agreement with the ones obtained by different methods.

Key words: MHD — galaxies: active — galaxies: jets

1 INTRODUCTION

It is now a generally accepted model that the ordered magnetic field in the vicinity of the supermassive black holes (SMBH), residing in the centres of active galactic nuclei (AGN), play the key role in launching relativistic jets (Blandford et al. 2019). It is the presence of a magnetic field that either threads the black hole ergosphere and establishes the Blandford–Znajek process (Blandford & Znajek 1977), responsible for the extraction of a BH rotational energy to supply the jet power (Tchekhovskoy et al. 2011), or launches a jet from a disc via Blandford–Payne mechanism (Blandford & Payne 1982). The Poynting flux at the jet base defines the maximum Lorentz factor, that can be achieved if all the energy of electromagnetic field is transformed into a plasma bulk motion kinetic energy (e.g., Beskin 2010).

Many efforts have been done to understand the magnitude and geometry of a jet magnetic field at different scales. Polarisation measurements in radio band yields us information about possible B-field geometry. Multiple studies at parsec scales reveal the helical magnetic field expected from the theoretical modelling (Gabuzda et al. 2017, 2018). The unprecedented radio images of M87 allowed to confirm that the helical magnetic field B is maintained at the scales from 300 pc up to 1 kpc (Pasetto et al. 2021). The observed Faraday rotation measure (RM) changing sign can be explained by the presence of toroidal magnetic field around a jet in 3C 273 up to the distances of order of 500 pc de-projected (Lisakov et al. 2021). The detection of a large scale toroidal magnetic

field at the kpc scales (Knuettel et al. 2017) indicates the strong electric current flowing in the relativistic jets far from the expected acceleration and collimation domain (Blandford et al. 2019; Kovalev et al. 2020), showing the importance of a Poynting flux even at such distances from the central engine. Direct polarimetry of the event horizon scales in M87 jet by Event Horizon Telescope Collaboration (2021) provides the B-field magnitude of the order of a few to tens Gauss.

One of the most robust methods to estimate the magnetic field amplitude on the observational basis is using the core shift measurements. The core shift effect is observed in jets due to the changing physical properties (flow velocity, magnetic field and emitting plasma number density) along an outflow, so that the surface with optical depth equal to unity appears at the different positions for the different observational frequencies (Lobanov 1998; Hirotani 2005). Together with the model assumptions, core shift measurements provide for the magnetic field typical values of the order of 1 G at 1 pc distance (Lobanov 1998). The results obtained using this method are in general agreement with other expected jet parameters, such as initial magnetisation and jet composition (Hirotani 2005; O’Sullivan & Gabuzda 2009; Zdziarski et al. 2015; Nokhrina et al. 2015; Pushkarev et al. 2012).

The core shift method as its important ingredients uses the following assumptions: equipartition between the proper frame emitting particles and magnetic field energy density, certain scalings with the distance of a magnetic field B and plasma number density n (Blandford & Königl 1979) and conical jet geometry. The observed jet boundary shape — the dependence of a jet width d on a distance along a jet r

* E-mail: nokhrinaelena@gmail.com

— can be approximated by the power-law

$$d = a_1 r^k. \quad (1)$$

The extensive study of jet shapes (see e.g. [Pushkarev et al. 2017](#), and references within) reveals in many sources approximately constant power $k \approx 1$, corresponding to a conical or quasi-conical geometry with index k being close to unity. However, recent studies of a dozen of nearby jets demonstrate, that their shapes are consistent with two power laws, smoothly transiting from one to another on more or less short scale of the overall length range ([Asada & Nakamura 2012](#); [Tseng et al. 2016](#); [Hada et al. 2018](#); [Akiyama et al. 2018](#); [Nakahara et al. 2018, 2019, 2020](#); [Kovalev et al. 2020](#); [Park et al. 2021](#); [Boccardi et al. 2021](#); [Okino et al. 2022](#)). For these sources the typical values of k closer to the jet launching point is $k \approx 0.39 - 0.59$. This we call quasi-parabolic, or parabolic for short. Further downstream the shape becomes closer to conical (quasi-conical) with $k \approx 0.73 - 1.4$ (e.g. [Asada & Nakamura 2012](#); [Boccardi et al. 2021](#); [Kovalev et al. 2020](#)). The implicit study of a geometry of the more distant sources shows that the cores at 15 and 8 GHz belong to a quasi-parabolic part of a jet ([Nokhrina et al. 2022](#)). This means that one may expect the radio cores observed at high frequencies 230 – 15 GHz and, may be, down to 8 GHz, being in a parabolic domain and with a plasma being still accelerated. This may impact the results by classical core shift method, which uses typical observational frequencies 8–15 GHz ([Pushkarev et al. 2012](#)).

Parabolic accelerating jet model alters the k_r -index in the frequency dependence of the core position $r_{\text{core}} \propto \nu^{-1/k_r}$ ([Ricci et al. 2022](#)). The multi frequency observations for M87 by [Hada et al. \(2011\)](#) and for 20 sources by [Sokolovsky et al. \(2011\)](#) demonstrate that k_r is indeed close to unity. This may be explained by either the conical jet model with a constant Lorentz factor Γ , which may be the case for the sample by [Sokolovsky et al. \(2011\)](#), or the quasi-parabolic accelerating jet model observed at the maximum Doppler factor ([Ricci et al. 2022](#)) for M87 jet with a clear quasi-parabolic shape. On the other hand, a dedicated search in NGC 315 by [Ricci et al. \(2022\)](#) yields the change in k_r index from 0.57 to 0.93 approximately at the jet shape transition point. Using different methods, [Kutkin et al. \(2014\)](#) found the exponent k_r in range 0.6–0.8 for quasar 3C 454.3. The typical k_r -indices for the MOJAVE sample is estimated to be approximately 0.83 by [Kravchenko et al. \(in preparation\)](#).

Accounting for parabolic accelerating jets alters the scalings of a magnetic field B and plasma number density n as functions of a distance from the central source r , introduces non-constant plasma bulk flow motion Lorentz factor Γ and changes the way of extrapolating the magnetic field amplitude down to the gravitational radius scales ([Ricci et al. 2022](#)). In this paper we modify the core shift method for parabolic jet boundary geometry and estimate the magnetic field amplitude at the gravitational radius for ten sources.

The paper is organised as follows. In Section 2 we present the model for magnetic field and emitting particles number density to obtain the possible core shift indices k_r for a parabolic accelerating jets. In Section 3 we discuss the relation between magnetic field and plasma number density and obtain the expressions to estimate both values. In Section 4 we review the data to estimate B . We discuss our results

and methods in Section 5. Finally, we summarise our work in Section 6.

2 FREQUENCY DEPENDENT APPARENT CORE SHIFT IN PARABOLIC ACCELERATING FLOW

Emission and opacity of a jet results from the emitting plasma population with assumed power-law energy distribution in the plasma proper frame, designated by the asterisk:

$$dn_{\text{syn}*} = K_{e*} \gamma^{-1-2\alpha} d\gamma, \quad \gamma \in [\gamma_{\text{min}}; \gamma_{\text{max}}], \quad (2)$$

where α is a power of a spectral flux in the optically thin regime: $S_\nu \propto \nu^{-\alpha}$. Here K_{e*} is an amplitude of the emitting plasma energy distribution:

$$n_{\text{syn}*} = \frac{K_{e*}}{2\alpha} \left(\frac{1}{\gamma_{\text{min}}^{2\alpha}} - \frac{1}{\gamma_{\text{max}}^{2\alpha}} \right) \approx \frac{K_{e*}}{2\alpha \gamma_{\text{min}}^{2\alpha}}. \quad (3)$$

The relation between the observational frequency ν and the local properties of a jet at the surface of peak spectral flux (it approximately coincides with the surface with the optical depth equal to unity) is as follows (e.g. Equation (21) in [Hirotani 2005](#)):

$$\left(\nu \frac{1+z}{\delta} \right)^{2.5+\alpha} = C_1(\alpha) \frac{1+z}{\delta} \frac{d}{\sin \theta} r_0^2 \nu_0 \left(\frac{e}{2\pi m c} \right)^{1.5+\alpha} \times K_{e*} B_*^{1.5+\alpha}. \quad (4)$$

Here m , e , c , r_0 are the electron mass and charge, the speed of light and the classical electron radius; $\nu_0 = c/r_0$; $C_1(0.5) = 2.85$ for $\alpha = 0.5$ ([Gould 1979](#)). The local jet width is d , the emitting electron number density amplitude is K_{e*} and the local magnetic field in the plasma proper frame is B_* . The jet viewing angle is θ , and a Doppler factor for a bulk Lorentz factor $\Gamma = (1 - \beta^2)^{-0.5}$ is

$$\delta = \frac{1}{\Gamma(1 - \beta \cos \theta)}. \quad (5)$$

In order to obtain the dependence of the core position on the observational frequency, we need to set the dependence of K_{e*} , B_* , Γ , d and δ on the distance along a jet r .

The typical frequencies for the core shift measurements are 1.4 – 43 GHz ([Kovalev et al. 2008](#); [Hada et al. 2011](#); [Sokolovsky et al. 2011](#); [Boccardi et al. 2021](#)), and may be as high as 86 and 230 GHz for M87 ([Doeleman et al. 2012](#); [Hada et al. 2016](#)). This means that either all the observational frequencies, or the highest ones may probe the jet in its parabolic accelerating domain. Thus, we assume here the jet shape is given by (1), with the fiducial value for power $k = 0.5$ for strictly parabolic outflow, and $k \approx 0.4 - 0.6$ for a quasi-parabolic one.

In general, we assume the power-laws $K_{e*} \propto r^{-k_n}$ and $B_* \propto r^{-k_b}$. Magnetic field in a jet is decomposed in a poloidal B_p and toroidal B_φ components. The toroidal component dominates the major part of a jet $r > R_L$, as there is a universal relation $B_\varphi = B_p r / R_L$ for a relativistic flow (see e.g. [Lyubarsky 2009](#)). However, as the velocity of bulk plasma motion is dominated by a poloidal component, the corresponding relation in the plasma proper frame between $B_{p*} \approx B_p$ and $B_{\varphi*} \approx \sqrt{B_p^2 - E^2}$ can be different. We focus on the domain, where jet plasma is still effectively accelerating. In this

case either the co-moving magnetic field is dominated by the poloidal component $B_p^2 \gg B_\phi^2 - E^2$ or both components in a plasma proper frame are comparable $B_p^2 \sim B_\phi^2 - E^2$ (Vlahakis 2004; Komissarov et al. 2009). In this case we adopt

$$B_* \approx B_p^2. \quad (6)$$

To keep the final expression as simple as possible we will not account here for the jet transversal structure. Thus, the conservation of the total magnetic flux defines the dependence of B_* on the distance r :

$$B_*(r) = B_{\zeta*} \left(\frac{r_\zeta}{r} \right)^{2k}, \quad (7)$$

where r_ζ is a distance at which we will estimate the magnetic field and emitting plasma number density. It is convenient to use $r_\zeta = 1$ pc except for the source with the jet shape break detected at the smaller distances, as NGC 315 (Boccardi et al. 2021; Ricci et al. 2022).

The plasma number density obeys the continuity equation and can be written as

$$n_{*1} d_1^2 c \Gamma_1 = n_{*2} d_2^2 c \Gamma_2 \quad (8)$$

for the steady state in the accelerating jet. Here subscripts 1 and 2 indicate two different crosscuts perpendicular to the jet axis. We expect that the jets are still effectively accelerating in the parabolic domain (Nokhrina et al. 2019; Kovalev et al. 2020; Nokhrina et al. 2020, 2022), and the plasma bulk motion Lorentz factor

$$\Gamma(d) = \rho \frac{d}{2R_L} \quad (9)$$

grows linearly with the jet radius $d/2$ and depends on the light cylinder radius R_L (Beskin & Nokhrina 2006; Komissarov et al. 2007; Lyubarsky 2009). The ideal linear acceleration $\Gamma \propto d$ is valid while the flow is still highly magnetised. In order to account for the slowing down of this Lorentz factor behaviour as the flow approaches the saturation state with the magnetisation equal to unity, we introduce the coefficient ρ . Using relation (A13) from Nokhrina et al. (2022) and the Table 1 from Nokhrina et al. (2019), we conclude that $\rho \approx 0.3 - 0.55$. Using (8) and (9) we obtain the following relation for emitting plasma number density amplitude:

$$K_{e*} = K_{e*\zeta} \left(\frac{r_\zeta}{r} \right)^{3k}. \quad (10)$$

Substituting (7) and (10) into (4) we obtain the relation for frequency dependent core position

$$r \propto \nu^{-1/k_r}. \quad (11)$$

For the different relations between viewing angle θ and local Lorentz factor Γ in Ricci et al. (2022), we obtain three different values of core shift exponent k_r . For $\theta \approx \Gamma^{-1}$ Doppler factor is approximately constant, and

$$k_r = \frac{k_n + (1.5 + \alpha)k_b - k}{2.5 + \alpha}. \quad (12)$$

For $k_n = 3k$ and $k_b = 2k$ core shift exponent does not depend on the index of emitting particles distribution α : $k_r = 2k$. If $\theta \ll \Gamma^{-1}$, Doppler factor is proportional to the Lorentz factor $\delta \approx 2\Gamma$, and

$$k_r = \frac{k_n + (1.5 + \alpha)k_b - (2.5 + \alpha)k}{2.5 + \alpha}. \quad (13)$$

Substituting exponents from (7) and (10) we obtain

$$k_r = k \frac{3.5 + \alpha}{2.5 + \alpha}. \quad (14)$$

This expression depends weakly on emitting particle distribution for a reasonable range of α (see, e.g., Gould 1979). For $\alpha = 0.5$ this exponent $k_r = 4k/3$. If $\theta \gg \Gamma^{-1}$ and $\delta \propto \Gamma^{-1}$, one gets

$$k_r = \frac{k_n + (1.5 + \alpha)k_b + (0.5 + \alpha)k}{2.5 + \alpha}. \quad (15)$$

For $k_n = 3k$ and $k_b = 2k$

$$k_r = k \frac{6.5 + 3\alpha}{2.5 + \alpha}, \quad (16)$$

which is equal to $k_r = 8k/3$ for $\alpha = 0.5$ and, again, in general depends on α very weakly. All the above results have been obtained by Ricci et al. (2022), but assuming the dominance of toroidal magnetic field in the collimation and acceleration region.

Obtained $k_r = 2k$ for $\theta \approx \Gamma^{-1}$ for a strictly parabolic power $k = 0.5$ provides $k_r = 1$, which coincides with the result for a conical outflow with a constant speed. For a number of sources it is supported by multi frequency measurements for a dozen of sources (Sokolovsky et al. 2011; Hada et al. 2011). However, for different quasi parabolic jet collimation profiles and different viewing angles, k_r may vary. The core shift exponent measurements for NGC 315 favour $\theta \ll \Gamma^{-1}$ and $k_r = 4k/3$ (Ricci et al. 2022).

It is convenient to use the core shift offset (Lobanov 1998)

$$\Omega_{r\nu} = 4.8 \times 10^{-9} \frac{\Delta r_{\text{mas}} D_L}{(1+z)^2} \left(\frac{\nu_1^{1/k_r} \nu_2^{1/k_r}}{\nu_2^{1/k_r} - \nu_1^{1/k_r}} \right) \text{ pc GHz}^{1/k_r}, \quad (17)$$

where Δr_{mas} is a measured core shift in mas for observational frequencies ν_1 and ν_2 for a source at the luminosity distance D_L and corresponding cosmological red shift z . The core-position offset measure depends on $K_{e*\zeta}$ and $B_{*\zeta}$. If the relation between $K_{e*\zeta}$ and $B_{*\zeta}$ is set, measured core shift allows estimating magnetic field and emitting particles number density (Lobanov 1998; Hirotani 2005; O'Sullivan & Gabuzda 2009; Nokhrina et al. 2015).

3 MAGNETIC FIELD ESTIMATES BASING ON CORE SHIFT EFFECT

The classical equipartition between emitting plasma and magnetic field $K_{e*} \propto B_*^2$ cannot hold everywhere anymore due to relations (7) and (10) being in contrast with the conical approach (see App. A). To relate $K_{e*\zeta}$ and $B_{*\zeta}$ we introduce the local magnetisation — a ratio of Poynting flux to the plasma bulk motion kinetic energy flux (see, e.g., Nokhrina et al. 2015):

$$\sigma = \frac{B_\phi^2 c / 4\pi}{n_* \Gamma m c^3}. \quad (18)$$

Setting $\sigma = 1$, which corresponds to $\Gamma = \Gamma_{\text{max}}/2$, and using the universal for relativistic flows relation between toroidal

and poloidal magnetic field components (e.g., [Vlahakis 2004](#); [Lyubarsky 2009](#); [Komissarov et al. 2009](#))

$$\frac{B_\varphi}{B_p} = \frac{d}{2R_L}, \quad (19)$$

we obtain

$$n_{*\sigma=1} = \frac{\Gamma_{\max}}{8\pi mc^2 \rho^2} B_{*\sigma=1}^2. \quad (20)$$

In order to relate plasma number density and magnetic field at the given distance ζ and the point $\sigma = 1$, we use (7) and (10). This provides the following relation of $n_{*\zeta}$ and $B_{*\zeta}$:

$$n_{*\zeta} = B_{*\zeta}^2 \frac{\Gamma_{\max}}{8\pi mc^2 \rho^2} \frac{d_\zeta}{d_{br}}. \quad (21)$$

Assuming that just a fraction $\eta \in (0; 1]$ of all the plasma emits, we set

$$K_{e*\zeta} = B_{*\zeta}^2 \frac{\eta \Gamma_{\max}}{8\pi mc^2 \rho^2} \frac{d_\zeta}{d_{br}}. \quad (22)$$

With the above relation, we are able to write the final expression for estimating the jet magnetic field using the core shift effect in the parabolic accelerating jet with $\delta \approx \text{const}$ ($k_r = 2k$):

$$B_{*\zeta} = 0.0137 \left[\left(\frac{\Omega_{r\nu}}{r_\zeta} \right)^{6k} \left(\frac{1+z}{\delta} \right)^2 \frac{1}{\sin^{6k-1} \theta} \times \right. \\ \left. \times \frac{\rho^2 d_{br}}{\eta \Gamma_{\max} d_\zeta^2} \right]^{1/4} \text{ G}. \quad (23)$$

In the expressions for magnetic field $B_{*\zeta}$ all the distances (r_ζ , d_ζ , d_{br} and R_L) are in parsecs. Compare it with the classical expression for a magnetic field in the plasma proper frame at a distance 1 pc from the jet base (e.g., [Lobanov 1998](#); [Hirotani 2005](#)):

$$B_{*1} = 0.025 \left(\frac{\Omega_{r\nu}^3 (1+z)^2}{\delta^2 \varphi \sin^2 \theta} \right)^{1/4} \text{ G}, \quad (24)$$

where φ is a conical jet intrinsic half-opening angle.

The expression for a magnetic field in a case of $\delta \approx 2\Gamma$ ($k_r = 4k/3$) can be written as:

$$B_{*\zeta} = 0.0137 \left[\left(\frac{\Omega_{r\nu}}{r_\zeta} \right)^{4k} \frac{(1+z)^2}{\sin^{4k-1} \theta} \frac{R_L^2 \rho^2 d_{br}}{\eta \Gamma_{\max} d_\zeta^4} \right]^{1/4} \text{ G}. \quad (25)$$

Although the case of $k_r = 8k/3$ ($\delta \propto \Gamma^{-1}$) is unlikely, basing on the current observations, we still present the expression for B :

$$B_{*\zeta} = 0.0097 \left[\left(\frac{\Omega_{r\nu}}{r_\zeta} \right)^{7k} \frac{(1+z)^2 (1 - \cos \theta)^2}{\sin^{8k-1} \theta} \times \right. \\ \left. \times \frac{\rho^2 d_{br}}{\eta \Gamma_{\max} R_L^2 d_\zeta^{1-k}} \right]^{1/4} \text{ G}. \quad (26)$$

For the domain of effectively accelerating outflow, the co-moving magnetic field is dominated by the poloidal component ([Vlahakis 2004](#); [Komissarov et al. 2009](#)). This makes it straightforward estimating both the total magnetic flux contained in a jet and extrapolating magnetic field down to the gravitational radius scale.

The total magnetic flux is estimated as

$$\Psi = \pi \left(\frac{d_\zeta}{2} \right)^2 B_{*\zeta}. \quad (27)$$

Using the magnetic flux conservation, we obtain the magnetic field amplitude at the gravitational radius scales:

$$B_g^{\text{par}} = B_{*\zeta} \left(\frac{r_\zeta}{r_g} \right)^{2k}. \quad (28)$$

4 MAGNETIC FIELD ESTIMATES

Below we apply the above relations to the sources with the measured jet shape and core shift. Additionally we use the black hole mass estimate to assess the magnetic field amplitude at the gravitational radius. The needed parameters are summarised in the Tables 1–3.

To calculate the parameter $\Omega_{r\nu}$ using the expression (17) we adopt the core shift measurements by [Pushkarev et al. \(2012\)](#) between the observational frequencies 15.4 and 8.1 GHz. We also set $k_r = 2k$, where power k in a parabolic regime was measured in [Kovalev et al. \(2020\)](#) (see Tables 2 and 4). For M 87 jet we use the core shift measurements reported by [Hada et al. \(2011\)](#). The core position dependence is

$$r(\nu) = (1.40 \pm 0.16) \nu^{-0.94 \pm 0.09} + (-0.041 \pm 0.012). \quad (29)$$

For the homogeneity of the results, we calculate the core shift between the pair of frequencies 8.1 GHz and 15.4 GHz (see Table 3) using this expression. The obtained by [Hada et al. \(2011\)](#) k_r index assumes the value $1.06^{+0.12}_{-0.09}$, and it is in good agreement with the relation $k_r = 2k$, corresponding to a constant Doppler factor result (12). We set the measured $k_r = 1.06$ for M 87 ([Hada et al. 2011](#)). For NGC 315 we use the recent results by [Ricci et al. \(2022\)](#). In particular, multi frequency measurements are consistent with $k_r = 0.57 \pm 0.17$ at 22–8 GHz, and $k_r = 0.92 \pm 0.01$ at 8–5 GHz. This result is in agreement with formula (14) $k_r = 4k/3$, with $4k/3 = 0.6$ for $k = 0.45$ ([Boccardi et al. 2021](#)). We adopt the core shift measurement by [Boccardi et al. \(2021\)](#) between the frequencies 15.4 and 8.4 GHz. For 3C273 the core shift was measured by [Okino et al. \(2022\)](#). We choose the pair 23.7 and 15.4 GHz as the closest to the frequency pair in other sources. We also adopt $k_r = 2k$, since the authors fitted the core shift with assumed $k_r = 1$. The opacity parameters are listed in the Table 3. Please, note, that $\Omega_{r\nu}$ here calculated with k_r , which differs from the unity. In order to check that the corresponding cores are indeed lying in a quasi parabolic domain, we calculated the positions of cores from a jet base at the high and low frequencies: r_{ν_2} and r_{ν_1} — listed in columns (7) and (8) of the Table 3. We see that these cores lie closer to a jet base, than the geometry break point position r_{break} (see column (5) in the Table 2).

The jet geometry data — the jet opening parameter a_1 , power k in a parabolic domain, the jet width at the break d_{br} and the position of a break r_{break} are presented in the Table 2.

The variability Doppler factors estimates are summarised in the column seven of Table 1 ([Hovatta et al. 2009](#)). To estimate the Doppler factor for M 87 jet we employ the maximum speed in the acceleration region measured by [Mertens et al. \(2016\)](#) $\Gamma \sim 3$ with the viewing angle $\theta = 18^\circ$ from [Nakamura](#)

Table 1. Parameters of the sources with a measured parabolic jet shape and the core shift.

Source	z	θ (deg)	θ reference	M ($\log M_{\odot}$)	M reference	δ	φ_{app} ($^{\circ}$)
(1)	(2)	(3)	(4)	(5)	(6)	(7)	(8)
0055+300	0.017	38.0	Ricci et al. (2022)	9.32	Boizelle et al. (2021)	...	6.9
0111+021	0.047	5.0	Kovalev et al. (2020)	9.3
0415+379	0.049	17.4	Pushkarev et al. (2017)	8.21	Torrealba et al. (2012)	2.9	7.9
0430+052	0.033	18.7	Pushkarev et al. (2017)	8.13	Woo & Urry (2002)	5.9	9.6
1226+023	0.158	3.3	Pushkarev et al. (2017)	8.41	Gravity Collaboration et al. (2018)	17.0	6.6
1228+126	0.004	18.0	Nakamura et al. (2018)	9.82	EHT Collaboration et al. (2019)	3.2*	12.0
1514+004	0.052	15.0	Kovalev et al. (2020)	7.3
1637+826	0.024	18.0	Kovalev et al. (2020)	8.78	Ferrarese & Ford (1999)	...	7.2
1807+698	0.051	7.3	Pushkarev et al. (2017)	8.51	Woo & Urry (2002)	1.1	10.6
2200+420	0.069	8.0	Pushkarev et al. (2017)	8.23	Woo & Urry (2002)	7.3	24.8

Note. The columns are as follows: (1) source name (B1950); (2) redshift (collected by Kovalev et al. 2020); (3) viewing angle; (4) viewing angle reference; (5) black hole mass; (6) black hole mass reference; (7) variability Doppler factor from Hovatta et al. (2009); (8) apparent opening angle at 15 GHz core by Pushkarev et al. (2017).

* For 1228+126 Doppler factor is based on the measured at parsec scales velocities by Mertens et al. (2016) and the viewing angle.

Table 2. Jet geometry parameters of the sources.

Source	Alias	k	d_{break} (pc)	r_{break} (pc)	a_1 (pc^{1-k})	geometry reference
(1)	(2)	(3)	(4)	(5)	(6)	(7)
0055+300	NGC 315	0.45	0.072	0.58	0.092	Boccardi et al. (2021); Ricci et al. (2022)
0111+021	UGC 00773	0.497 ± 0.077	0.28	27.31	0.179 ± 0.010	Kovalev et al. (2020)
0415+379	3C 111	0.468 ± 0.026	0.74	29.00	0.305 ± 0.011	Kovalev et al. (2020)
0430+052	3C 120	0.556 ± 0.070	0.29	5.77	0.202 ± 0.015	Kovalev et al. (2020)
1226+023	3C 273	0.66	3.0	274	0.223	Okino et al. (2022)
1228+126	M 87	0.57	1.2	43.4	0.07	Nokhrina et al. (2019)
1514+004	PKS B1514+004	0.564 ± 0.048	0.34	13.1	0.171 ± 0.019	Kovalev et al. (2020)
1637+826	NGC 6251	0.506 ± 0.041	0.16	3.3	0.155 ± 0.005	Kovalev et al. (2020)
1807+698	3C 371	0.388 ± 0.087	0.25	12.8	0.207 ± 0.016	Kovalev et al. (2020)
2200+420	BL Lac	0.537 ± 0.057	0.95	24.6	0.505 ± 0.029	Kovalev et al. (2020)

Note. The columns are as follows: (1) source name (B1950); (2) k -index upstream the jet shape geometry transition (parabolic flow); (3) jet width at the transition region; (4) jet shape break position from the jet base; (5) a_1 coefficient in a jet shape (parabolic flow); (6) reference for a jet geometry results.

Table 3. Opacity parameters of the sources and the locations of radio cores and jet shape break points.

Source	Δr (mas)	ν_1 (GHz)	ν_2 (GHz)	reference nuclear opacity	$\Omega_{r\nu}$ ($\text{pc GHz}^{1/k_r}$)	r_{ν_2} (pc)	r_{ν_1} (pc)
(1)	(2)	(3)	(4)	(5)	(6)	(7)	(8)
0055+300	0.420	8.4	15.4	Boccardi et al. (2021)	8.94	0.12	0.34
0111+021	0.137	8.1	15.4	Pushkarev et al. (2012)	2.15	1.57	3.00
0415+379	0.315	8.1	15.4	Pushkarev et al. (2012)	5.62	1.01	2.01
0430+052	0.075	8.1	15.4	Pushkarev et al. (2012)	0.729	0.19	0.35
1226+023	0.036	15.4	23.7	Okino et al. (2022)	2.76	4.36	6.04
1228+126	0.089	8.1	15.4	Hada et al. (2011)	0.113	0.028	0.051
1514+004	0.139	8.1	15.4	Pushkarev et al. (2012)	2.05	0.70	1.24
1637+826	0.210	8.1	15.4	Pushkarev et al. (2012)	1.70	0.37	0.69
1807+698	0.249	8.1	15.4	Pushkarev et al. (2012)	6.44	1.49	3.41
2200+420	0.032	8.1	15.4	Pushkarev et al. (2012)	0.645	0.37	0.66

Note. The columns are as follows: (1) source name (B1950); (2) core shift between the low and high frequencies; (3) low frequency; (4) high frequency; (5) reference for a core shift measurement; (6) core-position offset $\Omega_{r\nu}$ calculated using columns (2)–(4) and k_r from Table (4); (7) core position from the jet base at the high frequency assuming k_r from Table 4; (8) the same as column (7), but at the low frequency.

et al. (2018). For the sources with unknown Doppler factor we set it as $\delta = 1$ basing on relatively large viewing angles of these jets.

In order to compare the magnetic field estimates based on the model of parabolic accelerating jets (23) with the ones based on conical geometry (24), we use apparent opening angle measurements by Pushkarev et al. (2017). These angles reflect the jet geometry at 15 GHz core. For M87 jet we use the apparent opening angle $\varphi_{\text{app}} \approx 5^\circ$ reported by Mertens et al. (2016) on parsec scales. To obtain the intrinsic half-opening angles, we use the relation

$$\varphi = \varphi_{\text{app}} \sin \theta / 2. \quad (30)$$

Viewing angles are collected in Pushkarev et al. (2017). However, for M 87 we use the value $\theta = 18^\circ$ from Nakamura et al. (2018), and for NGC 315 — from Ricci et al. (2022).

We set the parameters $\eta = 0.01$, basing on the modelling of synchrotron emission of nonuniform jets (Frolova et al. 2023), and $\rho = 0.33$ (Nokhrina et al. 2022).

The results are presented in Table 4. Using the equation (23) and the measured parameters, we estimate the magnetic field $B_{*\zeta}^{\text{par}}$ at the distance ζ (see column(2)) from the jet base for a parabolic accelerating jets. The conical estimate $B_{*\zeta}^{\text{cone}}$ is presented in column (6) to compare the results. We observe that for all the sources except for 3C 273 the magnetic field at the given distance ζ is about several times smaller than the estimates based on the conical jet geometry.

Special attention must be given to NGC 315. As the core shift index k_r at high frequencies clearly points to the case $\theta \ll \Gamma^{-1}$, we should apply the formula (25). We adopt the light cylinder radius $R_L = 4.7 \times 10^{-4}$ pc, corresponding to $\Gamma_{\text{max}} = 20$, and calculate magnetic field at 0.2 pc using the relation (25). In this case $B_{*\zeta}$ and B_g are by the order of magnitude lower, than in the case of the relation (23).

5 RESULTS AND DISCUSSION

First of all, we observe, that the magnetic field estimates within a model of a parabolic accelerating jet is a few times smaller than that for a classical conical model (Lobanov 1998). The only exception is 3C 273 with the largest in the sample jet width at the break d_{br} .

These differences in a magnetic field calculated within two different models — conical with a constant velocity and quasi-parabolic accelerating flow — results from the two effects. The first one is the difference in a dependence of K_{e*} and B_* on the distance r . For the ideal parabolic power $k = 0.5$ magnetic field $B_* \propto r^{-1}$ as in the Blandford–Königl model. On the other hand, the emitting plasma number density amplitude $K_{e*} \propto r^{-1.5}$ decreases slower than in the flow with a constant Lorentz factor. In a majority of our sources only the first effect plays the role: the core shift parameter $\Omega_{r\nu}$ and the core positions r_{ν_2} and r_{ν_1} for $k_r \approx 1$ are close to their values for the non-accelerating conical outflow. Thus, if we observe the core of accelerating parabolic jet at the same frequency and distance, as in the conical case, than the expression $K_{e*} B_*^{1.5+\alpha}$, which defines the local opacity (see Equation (4)) must also be the same. But, as the plasma number density decreases slower with the distance, than the magnetic field amplitude must be lower to balance the larger plasma number density. The second effect is the possible difference

in the parabolic and conical core positions for a large enough departures of k_r from the unity. In this case both effects play the role. If we set in NGC 315 (005+300) $k_r = 1$, the core shift offset would be equal to $\Omega_{r\nu} = 2.56$ pc GHz, and the core positions $r_{\nu_1} = 0.27$ and $r_{\nu_2} = 0.50$ pc. These values are larger than the ones calculated with $k_r = 0.57$, and such a difference in their positions works in the same direction as the first effect, making the magnetic field estimate in a parabolic jet even smaller than in the conical one. In 3C 273 (1226+023) for $k_r = 1$ $\Omega_{r\nu} = 4.27$ pc GHz, $r_{\nu_1} = 3.13$, $r_{\nu_2} = 4.82$ pc. The cores are situated closer to the jet base than the ones in the model with $k_r = 1.32$. In this case there is an interplay between the effects of slower decrease of K_{e*} with a distance and needed higher amplitudes in both K_{e*} and B_* for the surface with the optical depth equal to unity to be situated farther from the jet origin.

The dominance of a poloidal magnetic field component in the accelerating parabolic jet domain provides a convenient and straightforward way to recalculate the magnetic field onto scales of the order of a gravitational radius. The results are presented in the tenth column in Table 4. For NGC 315 both the obtained values $B_g^{\text{par}} = 21$ and 480 G can be compared with the independent estimate based on an assumption of magnetically arrested disc launching a jet (Ricci et al. 2022). The estimate for $k_r = 2k$ is in excellent agreement with $B_{\text{MAD}} = 125 - 480$ G at the lower limit event horizon radius. On the other hand, the magnetic field, obtained assuming $k_r = 4k/3$, when recalculated to the upper limit magnetosphere radius $10.6 r_g$, has the value 2.5 G, which correspond very well to the independent magnetic estimate 5 – 18 G at this scale. The $B_g^{\text{par}} = 80$ G estimate for M 87 is corroborated by the EHT results $B \approx 1 - 30$ G in the very vicinity of a central BH (Event Horizon Telescope Collaboration 2021). The rest of the sources in the sample have amplitudes of a magnetic field at the gravitational radius of the order of $10^3 - 10^4$ G, with only 3C 273 reaching a few of 10^5 G due to relatively large core shift measured by Okino et al. (2022). The estimated total magnetic flux in a jet assumes the expected values of $10^{32} - 10^{35}$ G · cm².

The presented above results depend on the modelling parameters such as the assumed fraction η of emitting plasma, the coefficient ρ describing a deviation from the strictly linear acceleration, the maximum possible Lorentz factor Γ_{max} of a bulk plasma motion and Doppler factor δ unknown for several sources in the sample. Fraction $\eta = n_{\text{syn}}/n$ is the most weakly constrained parameter. It is estimated to be from the order of 1% basing on the particle-in-cell simulations (Sironi & Spitkovsky 2011; Sironi et al. 2013; Sironi & Spitkovsky 2014) and modelling synchrotron intensity maps from the stratified jets (Frolova et al. 2023) to the order of 100% in numerical modelling by Kramer & MacDonald (2021). Parameters ρ and Γ_{max} are usually better constrained. We can estimate Γ_{max} with the precision up to a factor of a few (see discussion in Nokhrina et al. 2019). Both numerical (Chatterjee et al. 2019) and analytical (Nokhrina et al. 2022) modelling provide about the same accuracy for $\rho \approx 0.2 - 1$. Finally, the Doppler factor is unknown for four of the sources in our sample and assumed to be a unity.

The dependence of estimates (23) and (25) on the unknown ratio of emitting to full plasma number density and Γ_{max} is very weak: as the 1/4 power. This means that even if all the plasma emits ($\eta = 1$ instead of 0.01), magnetic field esti-

Table 4. Estimates of magnetic field.

Source	ζ (pc)	k_r	Γ_{\max}	$B_{*\zeta}^{\text{par}}$ (G)	$B_{*\zeta}^{\text{cone}}$ (G)	$K_{e*\zeta}$ (cm ⁻³)	$\log_{10} \Psi$ (G cm ²)	Σ_ζ	B_g^{par} (G)
(1)	(2)	(3)	(4)	(5)	(6)	(7)	(8)	(9)	(10)
0055+300	0.2	0.57	20	0.52	0.75	1.2×10^4	34.3	0.11	480
0055+300	0.2	0.57	20	0.023	0.75	23	32.9	0.11	21
0111+021	1.0	0.994	50	0.18	0.53	1.4×10^4	34.2	0.12	$700 - 3.4 \times 10^4^*$
0415+379	1.0	0.936	50	0.073	0.25	270	34.8	0.095	4.4×10^3
0430+052	1.0	1.112	40	0.014	0.040	13	33.7	0.075	8.0×10^3
1226+023	1.0	1.32	30	0.16	0.13	45	33.9	2.8	4.8×10^5
1228+126	1.0	1.06	20	0.0082	0.012	0.35	32.5	0.95	80
1514+004	1.0	1.128	50	0.11	0.27	590	34.3	0.095	$1.3 \times 10^3 - 1.1 \times 10^5^*$
1637+826	1.0	1.012	40	0.059	0.18	330	34.1	0.052	2.3×10^3
1807+698	1.0	0.776	50	0.13	0.61	1.3×10^3	34.5	0.060	660
2200+420	1.0	1.074	50	0.018	0.048	12.8	34.2	0.12	5.1×10^3

Note. The columns are as follows: (1) source name (B1950); (2) distance at which we estimate the magnetic field; (3) power k_r of a core shift; (4) assumed maximum Lorentz factor (see details in [Nokhrina et al. \(2020\)](#) and [Ricci et al. \(2022\)](#)); (5) estimate of magnetic field at distance ζ ; we use the formula for a constant Doppler factor (23) everywhere except the second line of 0055+300 (NGC 315), where we use the relation (25); (6) magnetic field adopting the conical non-acceleration jet model (24) at the same distance ζ ; (7) emitting particles number density amplitude $K_{e*\zeta}$ calculated using the relation (22); (8) the total magnetic flux in a jet (27); (9) estimate for a standard ratio between magnetic field and emitting plasma energy density, which is assumed to be equal to unity for a conical jet model; (10) magnetic field at the gravitational radius scale in parabolic geometry (28).

* The magnetic field at the gravitational radius for the sources 0111+021 and 1514+004 is presented for boundary BH masses $10^8 - 5 \times 10^9 M_\odot$.

mates would increase by the factor of about 3. This would provide both estimates based on parabolic and conical geometry closer to each other. The same holds for the total magnetic flux Ψ and the magnetic field at the gravitational radius B_g^{par} . Magnetic field depends on the particular values of ρ and δ as a power 1/2. Thus, the larger than assumed $\delta = 1$ Doppler factors will lower the magnetic field estimate as $1/\sqrt{\delta} \approx 3$ for e.g. $\delta = 10$ instead of 1. Thus, even the extreme values of these parameters will affect the result for B within a factor of a few.

Errors in estimates for the magnetic field and emitting plasma number density arise from the observational errors in measured values Δr , θ , δ , d_{break} and from model assumed values η , ρ , Γ_{\max} . Typical errors in observational data are of the order of tens percent ([Pushkarev et al. 2012, 2017](#); [Kovalev et al. 2020](#)), with the major source being an error in Δr . The largest expected uncertainty of the model parameters is in the fraction of emitting plasma number density η . As we discussed above, it may lead to the drop in an estimate of $B_{*\zeta}^{\text{par}}$ up to 3.2 times. Thus, the results presented in column (5) must be treated as estimates with the accuracy up to, but no more, than a factor of a few.

The estimate $B_{*\zeta}^{\text{cone}}$ based on conical non-accelerating jet model (24) depends on the apparent intrinsic opening angle φ_{app} , which reflects the local jet width at $r_1 = 1$ pc. It is changing in the acceleration and collimation zone. We checked that accounting for the true jet width $a_1 r_1^k$ provides smaller jet width and at the distance r_1 , leading to effectively smaller φ and, thus, even larger estimate for $B_{*\zeta}^{\text{cone}}$. However, due to a weak dependence of B_{*1} on φ in (24), its value changes at most by a factor of two.

After substitution of the relation (22) between $K_{e*\zeta}$ and $B_{*\zeta}$ into equations (23) and (25), we obtain the dependence of $K_{e*\zeta}$ on the observed values such as δ , and the implied (modelling) parameters such as η and ρ . In case of $k_r = 2k$,

the emitting plasma number density depends on the parameters η , Γ_{\max} , d_{br} , ρ and δ as

$$K_{e*\zeta} = 9.23 \left(\frac{\Omega_{r\nu}}{r_\zeta} \right)^{3k} \frac{1+z}{\sin^{(6k-1)/2} \theta} \sqrt{\frac{\eta \Gamma_{\max}}{d_{\text{br}}}} \frac{1}{\rho \delta}. \quad (31)$$

For $k_r = 4k/3$ the expression for the emitting plasma number density amplitude is

$$K_{e*\zeta} = 9.23 \left(\frac{\Omega_{r\nu}}{r_\zeta} \right)^{2k} \frac{1}{d_\zeta} \frac{1+z}{\sin^{(4k-1)/2} \theta} \sqrt{\frac{\eta \Gamma_{\max}}{d_{\text{br}}}} \frac{R_L}{\rho}. \quad (32)$$

We see that $K_{e*\zeta}$ estimate would grow by the factor of 10 if all the plasma emits ($\eta = 100$ instead of 1). The dependence of $K_{e*\zeta}$ on the Doppler factor is even stronger. If we take for four sources, for example, $\delta = 10$ instead of 1, the estimate in emitting plasma number density will fall by the same factor 10. It is worth noting that the sources with assumed $\delta = 1$ have the largest estimates for emitting plasma number density. Using fiducial $\delta = 10$ would decrease these values much closer to the ones for the sources with observational estimates of Doppler factor.

The new relation between K_{e*} and B_* presented in this work $K_{e*} \propto B_*^2 d$ is very important since it differs from usually accepted equipartition

$$\frac{B_*^2}{8\pi} = \int_{\gamma_{\min}}^{\gamma_{\max}} mc^2 \gamma dn_{\text{syn}*} \approx K_{e*} mc^2 \Lambda. \quad (33)$$

Here $\Lambda = \ln(\gamma_{\max}/\gamma_{\min})$ for $\alpha = 0.5$, and we used in our calculations $\Lambda = 10$. If we assume this classical equipartition regime, than the core shift offset $\Omega_{r\nu}$ should depend on the distance along a jet, or, correspondingly, on the particular frequency pair. See the details in Appendix A.

The relation (22) means that while a jet is still accelerating, the ratio K_{e*}/B grows proportional to the jet width until the acceleration ceases. This is due to dependence of particle number density in a plasma proper frame on the local

Lorentz factor. As soon as the flow reaches almost constant Γ , the additional dependence on a jet width, connected with Γ , vanishes, and the relation between K_{e*} and B_*^2 assumes naturally the classical form (33). In order to get a feeling of difference from the classical equipartition, we calculate the values

$$\Sigma_\zeta = \frac{B_*^2}{8\pi mc^2 K_{e*} \Lambda} \quad (34)$$

(presented in the column 9 in Table 4), which should be equal to unity for a classical equipartition regime.

Equations (23), (25) and (26) are similar to the Equations (13), (14) and (15) by Ricci et al. (2022) with one important distinction. While the assumed dependence of both B_* and K_{e*} on r are the same in both works, the difference comes from the equipartition assumptions, and it affects the dependence of B_* on the d_ζ . Ricci et al. (2022) assumed $K_{e*\zeta} \propto B_{*\zeta}^2$ everywhere, and here we show that it is principal to set the relation $K_{e*\zeta} \propto B_{*\zeta}^2 d_\zeta$ for the consistency of the results (See Appendix A). This means that the Equations (13)–(15) by Ricci et al. (2022) can be applied for the comparable jet widths at the cores r_{ν_i} and at the point where we estimate the magnetic field ζ . Only in this case the obtained results are self-consistent. This condition holds for the for NGC 315 in Ricci et al. (2022), since $d_{\text{break}} = 0.072$, $d_{\nu_1} = 0.057$ and $d_{\nu_2} = 0.035$ pc. Extrapolating our magnetic field estimate from three distance $\zeta = 0.2$ pc to $\zeta = 0.58$ pc, we get $B_* = 0.2$ G, which is very close to the result 0.18 G by Ricci et al. (2022).

There is a zone along a jet, where the k -index changes more or less smoothly from quasi-parabolic value to quasi-conical. Observational data provides a change in k on the short length scales (see e.g. Kovalev et al. 2020; Boccardi et al. 2021), while the analytical modelling provides a wider range for such a change (Kovalev et al. 2020). Here we assume the constant k in a quasi parabolic domain, since the radio cores lie much closer to the jet origin than the geometry break position (see Tables 2 and 3). However, if the core at the lower frequency lies in the transition domain with the k -index being in between the parabolic and conical values, it will boost the magnetic field estimate closer to the results within the conical non-accelerating model.

6 SUMMARY

This work is dedicated to the modification of a core shift method developed by Lobanov (1998) for parabolic accelerating jets in the region of the observed radio cores. We apply our results to the sample of sources with the detected jet shape break. Our results are summarised as follows.

1. We use the poloidal component of a magnetic field as the dominant component B_* in the plasma proper frame. This is true for a still accelerating jet (Vlahakis 2004; Komissarov et al. 2009). We account for a changing particle number density in a plasma proper frame K_{e*} as the flow Lorentz factor grows. As a result, the relation between K_{e*} and B_*^2 deviates from the classical equipartition. The values of the core shift offset $\Omega_{r\nu}$ for different pairs of frequencies do not show any significant trend with r . It supports our using the relation (22) between K_{e*} and B_*^2 .

2. We show that for a jet boundary geometry given by

a power-law $d \propto r^k$ the core shift index in the parabolic accelerating jet may assume values $k_r = 2k$, $k_r = 4k/3$ and $k_r = 8k/3$ for $\theta \ll \Gamma^{-1}$ (Doppler factor $\delta \approx 2\Gamma$), $\theta \sim \Gamma^{-1}$ (Doppler factor $\delta \approx \text{const}$) and $\theta \gg \Gamma^{-1}$ (Doppler factor $\delta \propto \Gamma^{-1}$) respectively. Thus, for quasi parabolic jets, we should expect $k_r \approx 0.8 - 1.2$ and $k_r \approx 0.53 - 0.8$ for the most of the sources. Both values are observed (e.g., Hada et al. 2011; Sokolovsky et al. 2011; Porth et al. 2011; Kutkin et al. 2014), and we explain these values by the different viewing angles with respect to the emission opening angle $\sim \Gamma^{-1}$. In fact, this means, that multi frequency observations of radio cores coupled with the kinematics can provide one more instrument to constrain the jet viewing angle.

3. We obtained the formulas to estimate magnetic field B_* (23) and (25), and the emitting particles number density amplitude K_{e*} (22) using the measurements of a core shift effect and a jet geometry. We show that B_* can be straightforwardly used to calculate the magnetic field at the gravitational radius scales and the total magnetic flux in a jet. This is due to the dominance of a poloidal component in the accelerating jet region.

4. We have estimated a magnetic field in a jet B_* and on a gravitational radius B_g , a particle number density K_{e*} and a total magnetic flux Ψ for a sample of ten sources. The magnetic field at 1 pc distance along a jet is a few times smaller than the classical estimates. For NGC 315 we probed both equations (23) and (25), although the measured by Ricci et al. (2022) $k_r = 0.57$ strongly points to the case of $\theta \ll \Gamma^{-1}$. For M 87 and NGC 315 B_g can be compared with the independent estimates by different methods, and the correspondence is very good.

ACKNOWLEDGEMENTS

We thank the anonymous referee for suggestions which helped to improve the paper. This study has been supported by the Russian Science Foundation: project 20-72-10078, <https://rscf.ru/project/20-72-10078/>. This research made use of the data from the MOJAVE database¹ which is maintained by the MOJAVE team (Lister et al. 2018). This research made use of NASA’s Astrophysics Data System.

DATA AVAILABILITY

There is no new data associated with the results presented in the paper. All the previously published data has the proper references. Interferometric raw data of the project code BK134 is available from the VLBA archive².

REFERENCES

- Akiyama K., Asada K., Fish V., Nakamura M., Hada K., Nagai H., Lonsdale C., 2018, *Galaxies*, **6**, 15
- Asada K., Nakamura M., 2012, *ApJ*, **745**, L28
- Beskin V. S., 2010, *Physics Uspekhi*, **53**, 1199
- Beskin V. S., Nokhrina E. E., 2006, *MNRAS*, **367**, 375
- Blandford R. D., Königl A., 1979, *ApJ*, **232**, 34

¹ <http://www.physics.purdue.edu/MOJAVE/>

² <https://data.nrao.edu>

- Blandford R. D., Payne D. G., 1982, *MNRAS*, **199**, 883
- Blandford R., Znajek R., 1977, *MNRAS*, **179**, 433
- Blandford R., Meier D., Readhead A., 2019, *Annual Review of Astronomy and Astrophysics*, **57**, 467
- Boccardi B., et al., 2021, *A&A*, **647**, A67
- Boizelle B. D., et al., 2021, *ApJ*, **908**, 19
- Burbidge G., 1956, *ApJ*, **124**, 416
- Chatterjee K., Liska M., Tchekhovskoy A., Markoff S. B., 2019, *MNRAS*, **490**, 2200
- Doeleman S., Fish V., Schenck D., Beaudoin C., et al. 2012, *Science*, **338**, 355
- EHT Collaboration et al., 2019, *ApJ*, **875**, L1
- Event Horizon Telescope Collaboration 2021, *The Astrophysical Journal Letters*, **910**, L13
- Ferrarese L., Ford H. C., 1999, *ApJ*, **515**, 583
- Frolova V., Nokhrina E., Pashchenko I., 2023, *MNRAS*, **523**, 887
- Gabuzda D. C., Roche N., Kirwan A., Knuettel S., Nagle M., Houston C., 2017, *MNRAS*, **472**, 1792
- Gabuzda D. C., Nagle M., Roche N., 2018, *Astronomy & Astrophysics*, **612**, A67
- Gould R. J., 1979, *A&A*, **76**, 306
- Gravity Collaboration Sturm E., Dexter J., Pfuhl O., et al. 2018, *Nature*, **563**, 657
- Hada K., Doi A., Kino M., Nagai H., Hagiwara Y., Kawaguchi N., 2011, *Nature*, **477**, 185
- Hada K., Kino M., Doi A., Nagai H., et al. 2016, *ApJ*, **817**, 131
- Hada K., et al., 2018, *ApJ*, **860**, 141
- Hirofani K., 2005, *ApJ*, **619**, 73
- Hovatta T., Valtaoja E., Tornikoski M., Lähteenmäki A., 2009, *A&A*, **494**, 527
- Knuettel S., Gabuzda D., O’Sullivan S., 2017, *Galaxies*, **5**, 61
- Komissarov S. S., Barkov M. V., Vlahakis N., Königl A., 2007, *MNRAS*, **380**, 51
- Komissarov S. S., Vlahakis N., Königl A., Barkov M. V., 2009, *MNRAS*, **394**, 1182
- Kovalev Y., Lobanov A., Pushkarev A., Zensus J., 2008, *A&A*, **483**, 759
- Kovalev Y., Pushkarev A., Nokhrina E., Plavin A., Beskin V., Chernoglazov A., Lister M., Savolainen T., 2020, *MNRAS*, **495**, 3576
- Kramer J. A., MacDonald N. R., 2021, *A&A*, **656**, A143
- Kutkin A. M., et al., 2014, *MNRAS*, **437**, 3396
- Lisakov M. M., Kravchenko E. V., Pushkarev A. B., Kovalev Y. Y., Savolainen T. K., Lister M. L., 2021, *ApJ*, **910**, 35
- Lister M. L., Aller M. F., Aller H. D., Hodge M. A., Homan D. C., Kovalev Y. Y., Pushkarev A. B., Savolainen T., 2018, *ApJS*, **234**, 12
- Lobanov A. P., 1998, *A&A*, **330**, 79
- Lyubarsky Y., 2009, *ApJ*, **698**, 1570
- Mertens F., Lobanov A. P., Walker R. C., Hardee P. E., 2016, *A&A*, **595**, A54
- Nakahara S., Doi A., Murata Y., Hada K., Nakamura M., Asada K., 2018, *ApJ*, **854**, 148
- Nakahara S., Doi A., Murata Y., Nakamura M., Hada K., Asada K., 2019, *ApJ*, **878**, 61
- Nakahara S., Doi A., Murata Y., Nakamura M., Hada K., Asada K., Sawada-Satoh S., Kamenoi S., 2020, *AJ*, **159**, 14
- Nakamura M., Asada K., Hada K., et al. 2018, *ApJ*, **898**, 146
- Nokhrina E. E., Beskin V. S., Kovalev Y. Y., Zheltoukhov A. A., 2015, *MNRAS*, **447**, 2726
- Nokhrina E. E., Gurvits L. I., Beskin V. S., Nakamura M., Asada K., Hada K., 2019, *MNRAS*, **489**, 1197
- Nokhrina E. E., Kovalev Y. Y., Pushkarev A. B., 2020, *MNRAS*, **498**, 2532
- Nokhrina E. E., Pashchenko I. N., Kutkin A. M., 2022, *MNRAS*, **509**, 1899
- O’Sullivan S. P., Gabuzda D. C., 2009, *MNRAS*, **400**, 26
- Okino H., Akiyama K., Asada K., Gómez J. L., et al. 2022, *ApJ*, **940**, 65
- Paiano S., Landoni M., Falomo R., Treves A., Scarpa R., Righi C., 2017, *ApJ*, **837**, 144
- Park J., Hada K., Nakamura M., Asada K., Zhao G., Kino M., 2021, *ApJ*, **909**, 76
- Pasetto A., et al., 2021, *The Astrophysical Journal Letters*, **923**, L5
- Porth O., Fendt C., Meliani Z., Vaidya B., 2011, *ApJ*, **737**, 42
- Pushkarev A. B., Hovatta T., Kovalev Y. Y., Lister M. L., Lobanov A. P., Savolainen T., Zensus J. A., 2012, *Astronomy & Astrophysics*, **545**, A113
- Pushkarev A. B., Kovalev Y. Y., Lister M. L., Savolainen T., 2017, *MNRAS*, **468**, 4992
- Ricci L., et al., 2022, *Astronomy & Astrophysics*, **664**, A166
- Sironi L., Spitkovsky A., 2011, *ApJ*, **726**, 75
- Sironi L., Spitkovsky A., 2014, *ApJ*, **783**, L21
- Sironi L., Spitkovsky A., Arons J., 2013, *ApJ*, **771**, 54
- Sokolovsky K. V., Kovalev Y. Y., Pushkarev A. B., Lobanov A. P., 2011, *A&A*, **532**, A38
- Tchekhovskoy A., Narayan R., McKinney J. C., 2011, *MNRAS*, **418**, L79
- Torrealba J., Chavushyan V., Cruz-González I., Arshakyan T. G., Berton E., Rosa-González D., 2012, *Revista Mexicana de Astronomía y Astrofísica*, **48**, 9
- Tseng C.-Y., Asada K., Nakamura M., Pu H.-Y., Algaba J.-C., Lo W.-P., 2016, *ApJ*, **833**, 288
- Vlahakis N., 2004, *The Astrophysical Journal Letters*, **600**, 324
- Woo J. H., Urry C. M., 2002, *ApJ*, **579**, 530
- Zdziarski A., Sikora M., Pjanka P., Tchekhovskoy A., 2015, *MNRAS*, **451**, 927

APPENDIX A: POSSIBLE RELATIONS BETWEEN PLASMA NUMBER DENSITY AND MAGNETIC FIELD

Suppose there is some kind of relation between the emitting particles number density amplitude k_{e*} and the magnetic field B_* in the region of the observed radio cores. The usually used one is the equipartition between energy density of emitting plasma and magnetic field $k_{e*} \propto B_*^2$ (Burbidge 1956; Blandford & Königl 1979; Lobanov 1998). Suppose also, that the the multi frequency observations are indeed consistent with the power-law dependence (11), which means a constant (at least for the implied distances along a jet) $\Omega_{r\nu}$ (e.g., Sokolovsky et al. 2011; Hada et al. 2011). Let us discuss the possible relations between the emitting plasma number density and the magnetic field in the plasma proper frame, that ensure $\Omega_{r\nu}$ being approximately constant for different frequency pairs. The latter, in turn, means constant value at different distances r_ζ .

Substituting relations $K_{e*} \propto r^{-k_n}$, $B_* \propto r^{-k_b}$ and (1) into Equation (4), we obtain the following:

$$\Omega_{r\nu}^p = C r_\zeta^{k_n + k_b(1.5 + \alpha)} K_{e*} B_*^{1.5 + \alpha}, \quad (\text{A1})$$

where the power p and the coefficient C depend on assumed Doppler factor dependence on the Lorentz factor.

Case 1. Approximately constant Doppler factor δ .

$$p = k_n + k_b(1.5 + \alpha) - k, \quad (\text{A2})$$

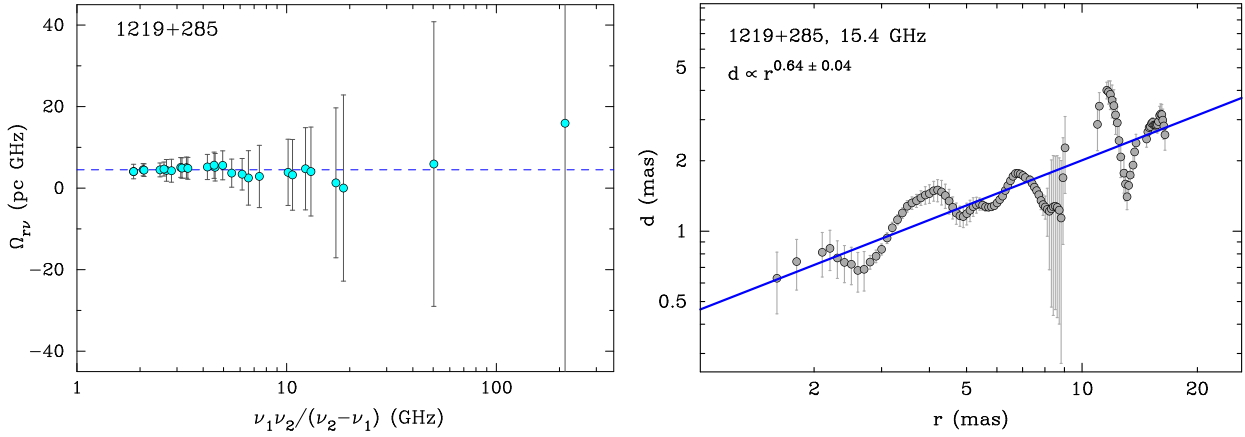


Figure A1. Left: Dependence of $\Omega_{r\nu}$ on a frequency parameter $\nu_1\nu_2/(\nu_2 - \nu_1)$ for BL Lacertae object 1219+285 constructed from VLBI observations at 1.4, 1.7, 2.3, 2.4, 4.6, 5.0, 8.1, 8.4 and 15.4 GHz. Dashed line denotes the median $\Omega_{r\nu}$. Smaller x-axis values correspond to wider frequency pairs and vice versa. Right: Evolution of the jet width as a function of the VLBI core separation at 15.4 GHz showing a quasi-parabolic streamline. Solid blue line represents the fitted dependency.

$$C = 3.086 \times 10^{-9(0.5+\alpha)} C_1(\alpha) r_0^2 \nu_0 \left(\frac{e}{2\pi mc} \right)^{1.5+\alpha} \times \left(\frac{\delta}{1+z} \right)^{1.5+\alpha} a_1 \sin^{p-1} \theta, \quad (\text{A3})$$

where r_0 , ν_0 , e are in CGS units, and a_1 – in pc^{1-k} .

Case 2. Doppler factor $\delta \approx 2\Gamma$.

$$p = k_n + k_b(1.5 + \alpha) - k(2.5 + \alpha), \quad (\text{A4})$$

$$C = 3.086 \times 10^{-9(0.5+\alpha)} C_1(\alpha) r_0^2 \nu_0 \left(\frac{e}{2\pi mc} \right)^{1.5+\alpha} \times \frac{\rho^{1.5+\alpha} a_1^{2.5+\alpha} \sin^{p-1} \theta}{(1+z)^{1.5+\alpha} R_L^{1.5+\alpha}}. \quad (\text{A5})$$

where R_L is in pc.

Case 3. Doppler factor $\delta \propto \Gamma^{-1}$.

$$p = k_n + k_b(1.5 + \alpha) + k(0.5 + \alpha), \quad (\text{A6})$$

$$C = 3.086 \times 10^{-9(0.5+\alpha)} C_1(\alpha) r_0^2 \nu_0 \left(\frac{e}{2\pi mc} \right)^{1.5+\alpha} \times \frac{\sin^{p-1} \theta}{a_1^{0.5+\alpha}} \left(\frac{2R_L}{\rho(1 - \cos \theta)(1+z)} \right)^{1.5+\alpha}. \quad (\text{A7})$$

where R_L in pc.

We see, that $\Omega_{r\nu}^p$ is proportional to the expression

$$K_{e*\zeta} B_{*\zeta}^{1.5+\alpha} r_\zeta^{k_n+k_b(1.5+\alpha)}, \quad (\text{A8})$$

which, in turn, we do not expect to depend on the particular distance along a jet ζ .

Suppose, the relation $K_{e*} \propto B_*^2$ holds together with $K_{e*} \propto r^{-k_n}$ and $B_* \propto r^{-k_b}$. If the expression (A8) does not depend on distance r_ζ , the following equality must be true:

$$k_n = 2k_b. \quad (\text{A9})$$

This equality is independent of the particular index of plasma energy distribution α . It holds, for an instance, for classical

approach (Lobanov 1998) with $k_n = 2$ and $k_b = 1$. However, it does not hold for the assumptions (7) and (10). The self-consistent dependence of $\Omega_{r\nu}$ on $K_{e*\zeta}$, $B_{*\zeta}$ and r_ζ exists only for a certain relations between emitting plasma number density and magnetic field. Suppose, one can relate the number density amplitude with the magnetic field as

$$K_{e*\zeta} \propto B_{*\zeta}^l r_\zeta^m. \quad (\text{A10})$$

In order the combination (A8) does not depend on ζ , the following relation between exponents l and m must hold:

$$k_n + m = k_b l. \quad (\text{A11})$$

In expression (21) $l = 2$ and $m = k$, so the condition (A11) is indeed fulfilled, and it has an underlying clear physical meaning, as described in section 4. This relation holds for any dependence of the Doppler factor δ on Γ , i.e. for any relation between the viewing angle θ and Lorentz factor Γ , as long as expressions (7) and (10) hold.

To examine whether there is significant trends of $\Omega_{r\nu}$ with r , we analysed the very long baseline interferometry (VLBI) observations of 20 pre-selected sources carried out during four 24h sessions between March and June 2007 (project code BK134) aimed on core shift analysis (Sokolovsky et al. 2011). The observations were performed simultaneously at nine frequencies, ranging from 1.4 to 15.4 GHz, thus forming both narrow and wide frequency pairs and enabling us to probe different spatial scales of the inner jet regions of the target sources. In Figure A1 (left), we show that $\Omega_{r\nu}$ is quite stable for the relatively close, $z = 0.107$ (Paiano et al. 2017), i.e. the luminosity distance $D_L = 465$ Mpc, BL Lacertae object 1219+285 (W Comae), assuming $k_r = 1$. We note that the inner jet shape of the source is quasi-parabolic (Figure A1, right), as inferred from the observations at the highest frequency of 15.4 GHz by analysing profiles transverse to the total intensity ridgeline of the outflow that we constructed following the procedure described in Pushkarev et al. (2017) in detail. Among the other 19 sources characterised by different inner jet shapes, such as quasi-parabolic and quasi-conical, a similar flat frequency dependence on $\Omega_{r\nu}$ is observed.

This paper has been typeset from a $\text{\TeX}/\text{\LaTeX}$ file prepared by the author.